http://www.kidney-international.org

Hemodynamic wall shear stress profiles influence the magnitude and pattern of stenosis in a pig AV fistula

Mahesh K. Krishnamoorthy[1], Rupak K. Banerjee[1,5], Yang Wang[2], Jianhua Zhang[2], Abhijit Sinha Roy[2], Saeb F. Khoury[3], Lois J. Arend[4], Steve Rudich[2] and Prabir Roy-Chaudhury[2,5]

[1]Cincinnati Dialysis Access Research Program, Department of Mechanical, Industrial, and Nuclear Engineering, University of Cincinnati, Cincinnati, Ohio, USA; [2]Cincinnati Dialysis Access Research Program, Division of Nephrology, University of Cincinnati, Cincinnati, Ohio, USA; [3]Cincinnati Dialysis Access Research Program, Division of Cardiology, University of Cincinnati, Cincinnati, Ohio, USA and [4]Cincinnati Dialysis Access Research Program, Department of Pathology, University of Cincinnati, Cincinnati, Ohio, USA

Venous stenosis is a significant problem in arteriovenous fistulae, likely due to anatomical configuration and wall shear stress profiles. To identify linkages between wall shear stress and the magnitude and pattern of vascular stenosis, we produced curved and straight fistulae in a pig model. A complete wall stress profile was calculated for the curved configuration and correlated with luminal stenosis. Computer modeling techniques were then used to derive a wall shear stress profile for the straight arteriovenous fistula. Differences in the wall shear stress profile of the curved and straight fistula were then related to histological findings. There was a marked inverse correlation between the magnitude of wall shear stress within different regions of the curved arteriovenous fistula and luminal stenosis in these same regions. There were also significantly greater differences in wall shear stress between the outer and inner walls of the straight as compared to curved arteriovenous fistula, which translated into a more eccentric histological pattern of intima-media thickening. Our results suggest a clear linkage between anatomical configuration, wall shear stress profiles, and the pattern of luminal stenosis and intima-media thickening in a pig model of arteriovenous fistula stenosis. These results suggest that fistula failure could be reduced by using computer modeling prior to surgical placement to alter the anatomical and, consequently, the wall shear stress profiles in an arteriovenous fistula.

Kidney International (2008) **74,** 1410–1419; doi:10.1038/ki.2008.379; published online 24 September 2008

KEYWORDS: AV fistula configuration; computational fluid dynamics; hemodialysis vascular access dysfunction; hemodynamics; wall shear stress

Correspondence: *Prabir Roy-Chaudhury, Cincinnati Dialysis Access Research Program, Division of Nephrology, University of Cincinnati, MSB G251, 231 Albert Sabin Way, Cincinnati, Ohio 45267-0585, USA.*
E-mail: Prabir.roychaudhury@uc.edu

[5]These authors contributed equally to this work.

Received 17 September 2007; revised 23 April 2008; accepted 6 May 2008; published online 24 September 2008

Over the past few years there has been a concerted effort both at the national (Fistula First) and local levels to increase the incident and prevalent rate of arteriovenous (AV) fistulae in view of better survival of this mode of access as compared to dialysis access grafts.[1–5] This much needed push to increase the prevalence of AV fistulae, however, has resulted in aggressive fistula placement in patients at higher risk for fistula failure and the use of surgical techniques (transpositions) with lower success rates.

Although, the reasons for primary failure or 'failure to mature' are not clearly understood, a number of clinical studies have demonstrated that an angiographic evaluation (usually within 3 months) in patients whose fistulae have not matured adequately to support hemodialysis, invariably documents vascular stenoses (usually within the first 5 cm of the venous segment.[2,6–8] We have more recently demonstrated that at least some of these AV fistulae fail as a result of aggressive neointimal hyperplasia.[9] Possible reasons for this venous stenosis include anatomical configuration and hemodynamic shear stress profiles within the venous segment. Although preexisting arterial stenoses, which become hemodynamically significant only after AV fistula creation could possibly result in the inability of the veins to mature, they do not cause venous stenosis. The described studies will focus on the former two issues.

At a physiological level, the anastomosis of an artery to a vein results in a very rapid increase in flow and consequently in WSS (wall shear stress) within both the artery and vein.[10,11] Since vessels always try and maintain WSS levels within the normal range this results in a rapid dilatation of the vein, which returns WSS levels to normal.[12,13] Indeed at an experimental level, high levels of WSS result in large luminal diameters due to vascular dilatation and lack of neointimal hyperplasia, while low levels of WSS results in small luminal diameters due to lack of vascular dilatation and the presence of neointimal hyperplasia.[14]

Regardless of the exact pathology that is present in these nonmaturing fistulae, we hypothesize that the driving force that determines whether a fistula will or will not mature, is

the hemodynamic WSS that is present soon after AV fistula placement. Specifically, we believe that the anatomical configuration will have a significant impact on the WSS levels and consequent fistula maturation or stenosis. The aim of the current study, therefore, was to (1) establish correlations between WSS profiles at the time of surgery and percentage luminal stenosis at the time of killing within different regions of a 'curved' AV fistula, (2) alter the computational model of the curved configuration in order to obtain a straight configuration and hence derive the WSS profile for a straight AV fistula configuration, and (3) establish the impact of differences in the observed WSS patterns in the curved (calculated) and straight (derived) AV fistulae on the histological pattern of intima-media thickening in these two configurations.

RESULTS

Development of a calculated computational fluid dynamic model for the curved AV fistulae

Flow measurements. The average volume flow rate of blood was 780, 130, and 650 ml/min in the proximal artery (PA), distal artery (DA), and venous segment, respectively, thus demonstrating the attainment of flow balance in the AV fistula circuit of the curved AV fistula model (Figure 1). The measured pulsatile flow data was fitted using a Fourier series and averaged over one cycle to get a single volume flow rate as shown in Figure 2a with systole occurring at 0.18 s (t1) and diastole at 0.62 s (t2).

Pressure measurements. The mean direct pressure measurements in the PA and in the venous segment on day 2 were 53 and 28 mm Hg, respectively. The proximal venous pressure (mean = 28 mm Hg) was averaged as mentioned above over a single cardiac cycle and was applied as a boundary condition at the venous outlet (Figure 2b). Figure 2c explains clearly the boundary conditions applied to calculate the WSS profiles.

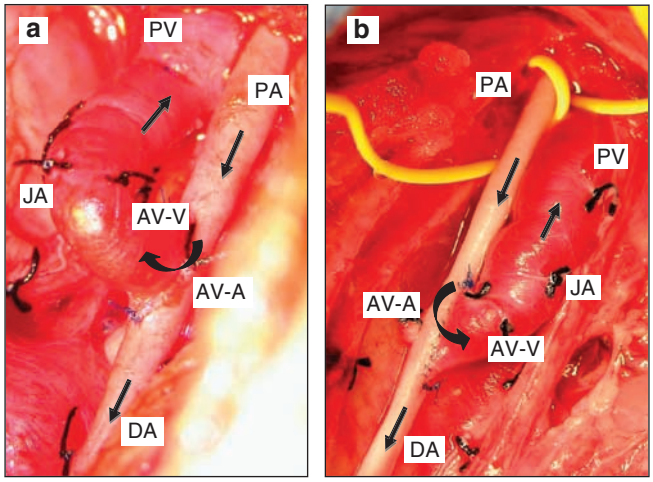

Figure 1 | Curved and straight AV fistula configurations in a pig showing different anatomical regions. (**a**, **b**) Curved and straight AV fistula configurations created in a pig model. The different anatomical regions are shown, namely PA, proximal artery; DA, distal artery; AV-A, arterial portion of AV anastomosis; AV-V, venous portion of AV anastomosis; JA, juxtaanastomotic segment; PV, proximal vein. The arrows denote the direction of the flow of blood.

Calculated WSS profiles for the curved AV fistula configuration. Figure 3 describes the three-dimensional mesh configuration (Gambit; Version 2.3.1) obtained from the intravascular ultrasound (IVUS) analyses. Addition of flow data into this model using finite volume method[15,16] (Fluent; Version 6.3.26), resulted in the development of a complete calculated WSS profile for the curved AV fistula configuration as shown in Figure 4.

Validation of the CFD model. To check the accuracy of our results and thereby to validate our computational model, we calculated Q_3^N and P_1^N (superscript N represents numerical), to compare with Q_3 and P_1 that were measured from *in vivo* experiments (Figure 2c). Flow rate balance was achieved in the curved AV fistula model. The PA pressure obtained from the computational fluid dynamic (CFD) model was 51 mm Hg as compared to 53 mm Hg that was obtained *in vivo* with a difference of less than 10% difference between the experimental and computational results of the pressure measurement.

Correlations between WSS profile and percentage luminal stenosis in the curved AV fistula

Figure 4 describes qualitatively the WSS contours in the curved AV fistula configuration. The WSS profiles as indicated by the contours show that there is a clear decrease in the values from AV anastomosis to the proximal vein (PV; from more red (high WSS) to more blue (low WSS)). Moderate levels of WSS values were observed in the juxtaanastomotic segment. In Figure 5, the WSS is quantified and correlated with the amount of luminal stenosis in the curved AV fistula. Figure 5a displays the WSS values averaged along the circumference of the cross-sections in different regions of the curved AV fistula. The mean WSS value decreases from AV anastomosis to PV, which correlates inversely with the magnitude of stenosis (intima-media thickening) in these same regions, which is shown in Figure 5b. Figure 5c represents the correlation between the mean WSS (dyn/cm^2) and the percentage luminal stenosis; with the correlation coefficients for the systolic and diastolic flow being 0.97 and 0.90, respectively. Thus, the WSS values at systole and diastole appear to have a strong inverse correlation with percentage luminal stenosis.

Development of a derived WSS profile for a straight configuration AV fistula and identification of differences between WSS profiles in the derived straight AV fistula as compared to the original curved AV fistula

Development of a derived WSS profile for a straight AV fistula configuration. Figure 6 describes the conversion of a curved AV fistula configuration into a straight AV fistula configuration, whereas Figure 7e describes the derived WSS in the straight AV fistula.

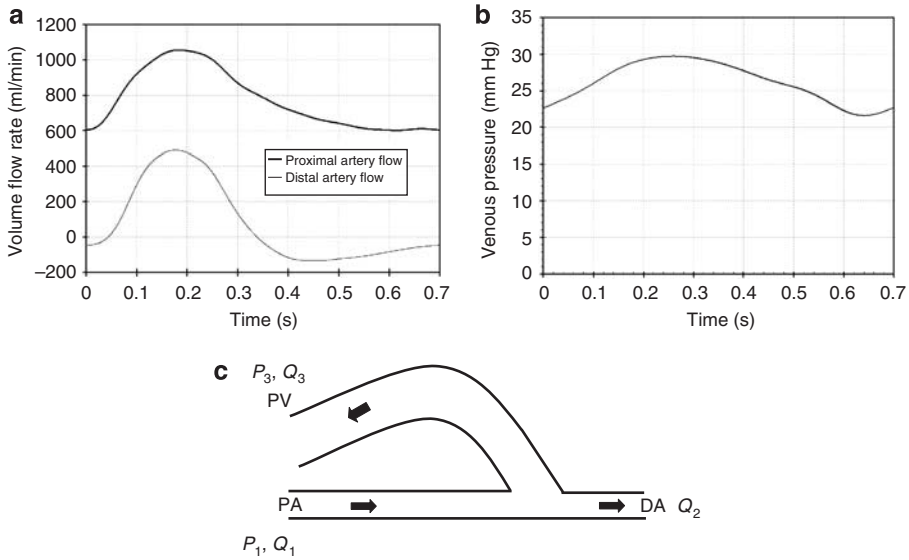

Figure 2 | Transient flow and pressure pulses measured *in vivo*. (**a**) Transient flow pulse in the proximal and distal artery in the curved fistula configuration, (**b**) the proximal venous pressure pulse in the curved fistula configuration. (**c**) The boundary conditions that were applied to the computational model in order to calculate the WSS profile for the AV fistulae. Specifically, transient pressure and flow pulses P_1, Q_1, respectively, were measured in the PA and transient flow pulse Q_2 was measured in the DA. Transient pressure and flow pulses P_3, Q_3, respectively, were measured in the PV. Only Q_1 (**a**), Q_2 (**a**), and P_3 (**b**) were applied as boundary conditions to obtain the WSS profile.

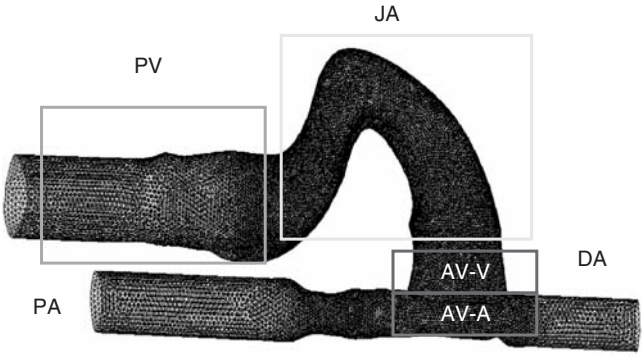

Figure 3 | Three-dimensional computational model of the AV fistula showing different anatomical regions. PV, proximal vein; JA, juxtaanastomotic region; AV-V, venous portion of the AV anastomosis; AV-A, arterial portion of the AV anastomosis.

Identification of differences between WSS profiles in the derived straight AV fistula as compared to the original curved AV fistula. Velocity profiles and values for WSS were calculated at 3 cm (cross-section 1) and 2.7 cm (cross-section 2) from the AV anastomosis for both the derived straight and experimental curved AV fistulae. The inner and outer wall locations for this cross-section were named as inner 1, inner 2, and outer 1, outer 2, respectively. Figure 7 shows the velocity vectors for both the curved (Figure 7b) and straight (Figure 7d) fistula configurations at an arbitrary location, which was different from either of the cross-sections 1 and 2. The main reason for describing the flow patterns and WSS profile in Figure 7 was to demonstrate the differences between the curved and straight configurations. The straight configuration (Figure 7d) shows a large difference in the velocity magnitude between the outer and inner wall as compared to the curved configuration (Figure 7b). There is also a significant amount of recirculation seen in the case of straight configuration (denoted by asterisk in Figure 7d). These differences in the velocity magnitude and the flow pattern translate into differences in WSS, which are shown in Figures 7c and 7e. Figure 7c describes the calculated overall WSS profile for the *in vivo* curved configuration, whereas Figure 7e describes the same for the derived straight configuration at peak flow during the cardiac cycle. It can be observed that the straight configuration experiences larger differences in WSS between the outer and inner wall (white and black circles) as compared to the curved configuration.

Figure 8 shows the comparison of WSS variations at the outer and inner walls for the straight and curved configurations at peak flow during the cardiac cycle. At cross-section 1, the net difference in the WSS values between the locations outer 1 and inner 1, for the curved configuration is 65.32 dyn/cm^2 (−7.12 dyn/cm^2 at outer 1 and 58.2 dyn/cm^2 at inner 1). In comparison, the net difference between the WSS values at outer 1 and inner 1 for the straight configuration is 135.9 dyn/cm^2 (114.9 dyn/cm^2 at outer 1 and −21 dyn/cm^2 at inner 1). Thus, the net difference in WSS values between the outer and inner locations at cross-section 1 increases by 108% in the case of the derived straight configuration as compared to the calculated *in vivo* results for the curved configuration. A similar shift occurs at cross-section 2. It is also important to note that, in the case of the straight configuration, the inner wall has a negative WSS value at cross-sections 1 and 2, whereas in the case of the curved configuration, the inner wall has a positive WSS stress value at these same points. A similar paradigm exists for the

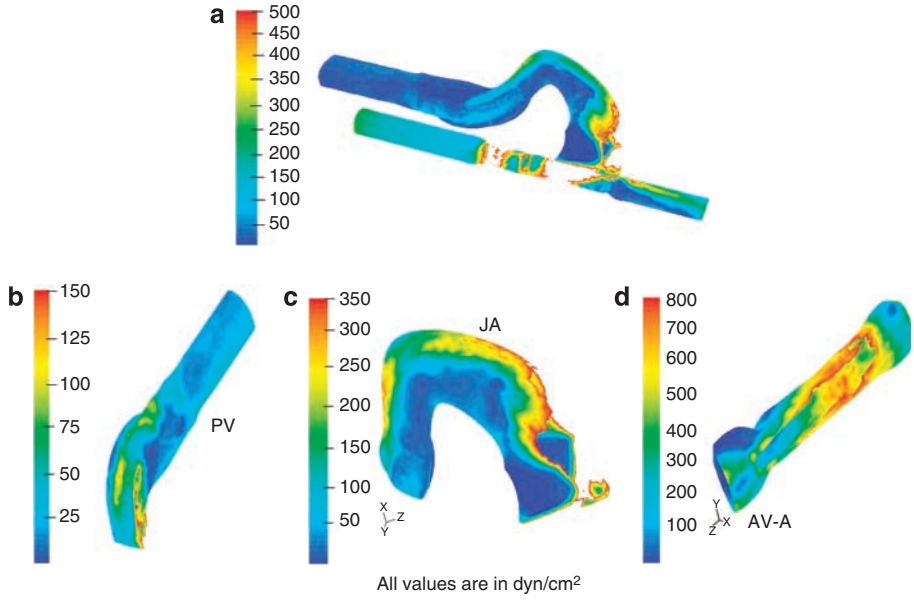

Figure 4 | Wall shear stress contours of curved AV fistula configuration during peak flow. (**a**) The WSS contours in the overall curved configuration. (**b–d**) The WSS contours in the different anatomical regions: PV, JA, and AV anastomosis, respectively.

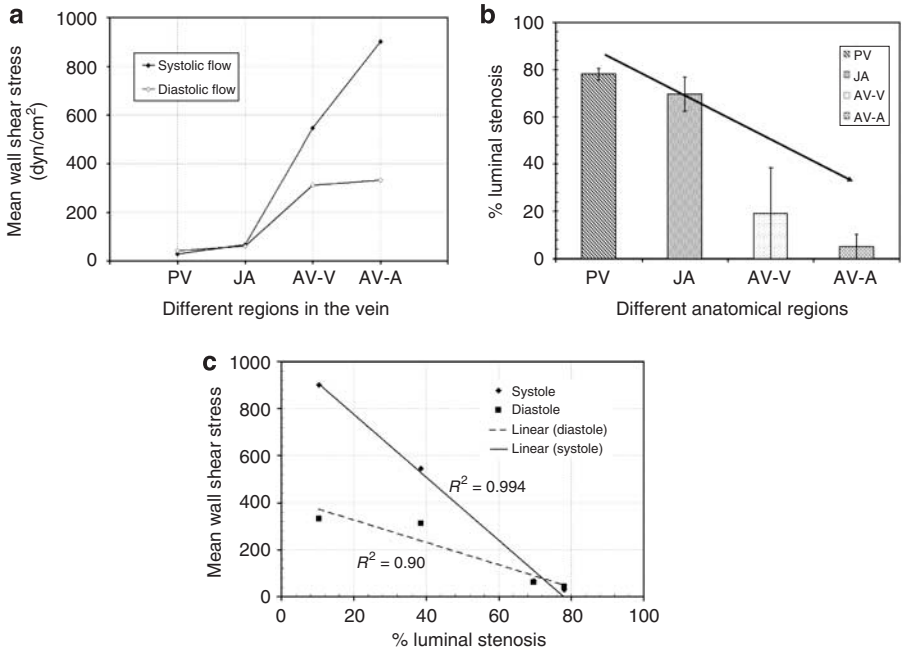

Figure 5 | Correlation of mean wall shear stress and percentage luminal stenosis in curved AV fistula configuration. (**a**) Mean wall shear stress in PV, JA, AV-V, and AV-A at systole and diastole. (**b**) Luminal stenosis at different anatomical regions of the curved AV fistula at 42 days postsurgery. Maximal stenosis (intima-media thickening) in this model occurs in the proximal vein (PV), with lesser degrees of stenosis in the juxtaanastomotic segment (JA), the venous side of the AV anastomosis (AV-V), and the arterial side of the AV anastomosis (AV-A), respectively, thus demonstrating an inverse correlation between WSS and luminal stenosis. (**c**) Represents the correlation between mean WSS and percentage luminal stenosis at 42 days postsurgery. The WSS values at both systole and diastole appear to correlate inversely with the percentage luminal stenosis.

outer wall, with a positive WSS value in the straight configuration at sections 1 and 2 and a negative value for the outer wall in the curved configuration. These differences are due to the extended curvature of the curved configuration, which results in organized Dean vortices at the curvature. These are caused by an elevation in the transverse velocity and momentum transfer in the radial direction, which results in reduced variation in WSS along the inner and outer walls of the vein section for the curved configuration. In marked contrast, the reduced radial

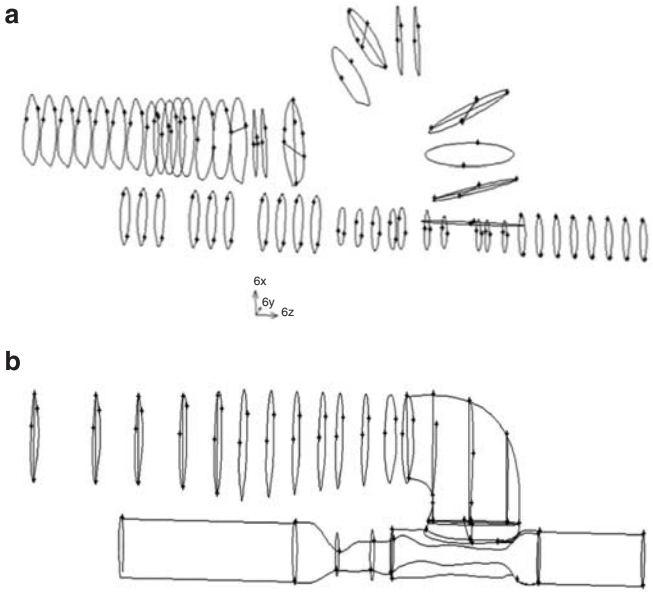

Figure 6 | Model reconstruction of straight fistula from curved fistula configuration. Representative digitized IVUS images for the proximal artery, proximal vein, and the AV anastomosis were used to construct the 3D geometry. Circular polylines obtained from the IVUS images of the (**a**) curved configuration were then altered to generate a (**b**) new "straight" anatomical profile with minimized venous curvature, which was then used to generate a "new" 3D straight AV fistula model.

curvature of the vein in the straight configuration leads to a higher axial momentum on one side of the vein as compared to the other side with less-organized Dean vortices. Therefore, the WSS in the axial direction remains high at the outer wall and less at the inner wall. Finally, in addition to the larger absolute difference between the outer and inner walls for the straight configuration as compared to the curved configuration, the straight configuration also had the greatest negative WSS values along its inner curve at these two cross-sections.

Figures 9a (curved) and 9b (straight) describes the spatial distribution of WSS at different distances from the AV anastomosis at peak flow during the cardiac cycle. In both these figures, the WSS values are plotted along a line through the midsection of the inner and outer walls of the curved and straight configurations, from the AV anastomosis (origin) to the vein outlet. Figure 9 documents that the absolute difference in WSS between the outer and inner walls is far greater for the straight as compared to the curved configuration at sections 1 and 2 (compare the magnitude of the double-headed arrows in the curved configuration to the double-headed arrows in the straight configuration). Figure 9 also demonstrates the inverse relationship between WSS values at the outer and inner walls for the curved and straight configurations at cross-sections 1 and 2, which was previously described in Figure 8. The two cross-sections 1

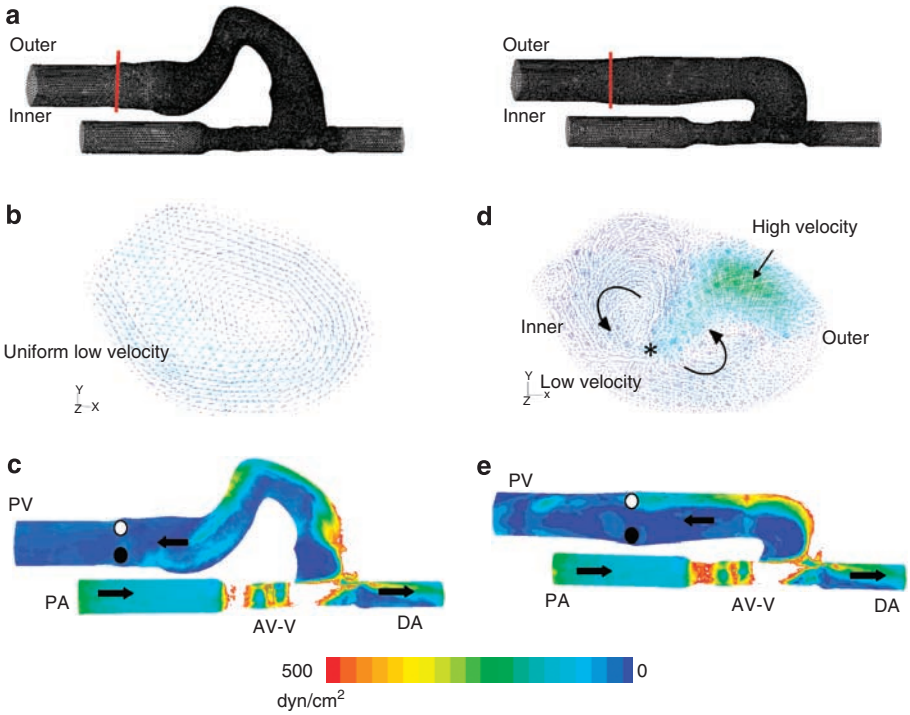

Figure 7 | Comparison of hemodynamics in curved and straight configuration. (**a**) Curved and straight AV fistula configurations showing the location of inner and outer walls and the location of cross-section along which the velocity vectors are plotted. (**b**, **d**) The velocity vectors at an arbitrary cross-section are different from cross-sections 1 and 2. Note the small differences in velocity flow pattern along the inner and outer walls for the (**b**) curved configuration as opposed to large differences in velocity profile and magnitude along the inner and outer walls for the (asterisk, **d**) straight configuration, with significant amounts of recirculation. (**c**) WSS contour for the curved configuration, (**e**) similar data for the straight configuration. The arrows denote the blood flow direction. Note that WSS values in the proximal vein beyond the curve appear to be lower in the curved configuration as compared to the straight configuration (circles with diagonals in (**c**, **e**)).

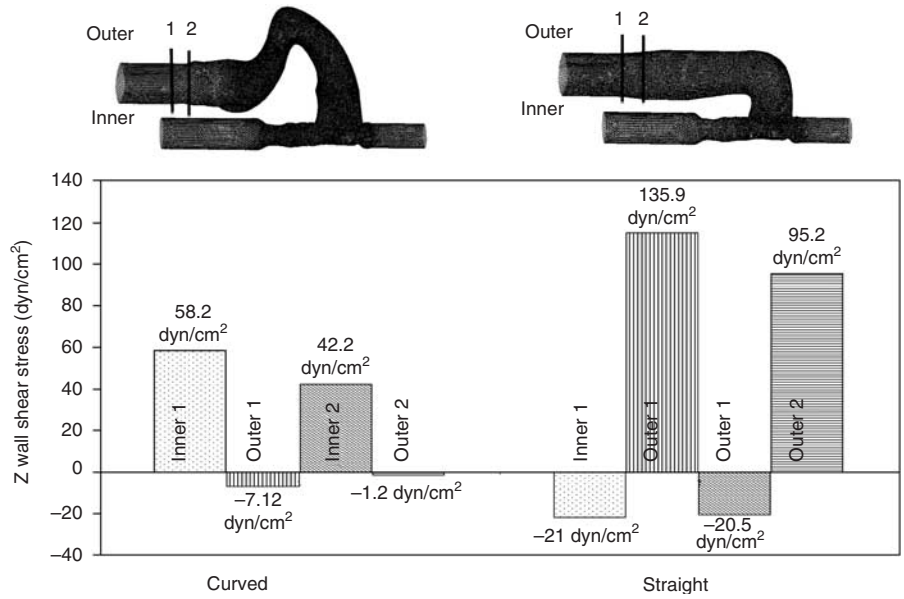

Figure 8 | Local wall shear stress variation with time at outer and inner walls. WSS variation at two venous cross-sections 1 and 2 that are 3 and 2.7 cm from the AV-anastomosis at the outer and inner wall locations during peak flow for curved and straight configurations. Note that the straight configuration has a negative WSS value at cross-sections 1 and 2 at the inner wall whereas the curved configuration has a positive WSS value at these same points on the inner wall. A similar paradigm exists for the outer wall, with a positive WSS value in the straight configuration at cross-sections 1 and 2 and a negative value for the outer wall in the curved configuration.

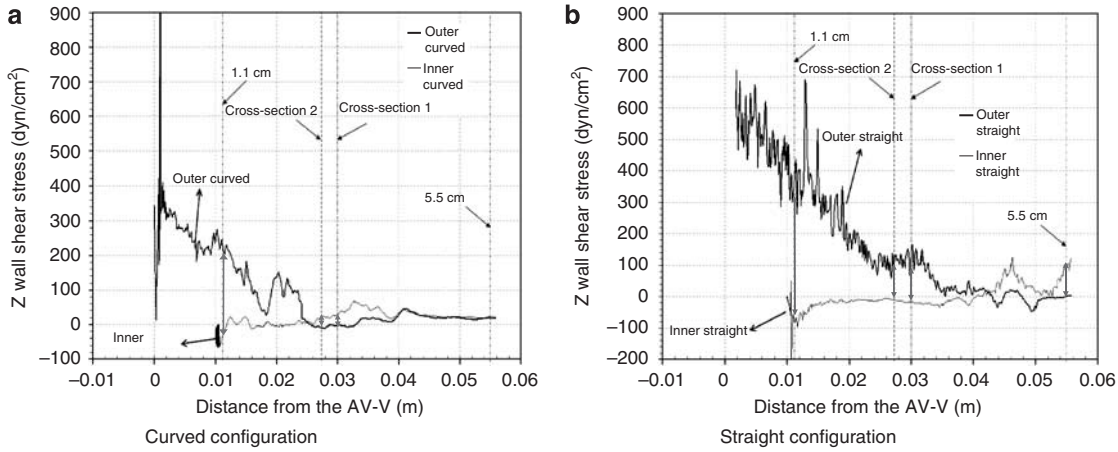

Figure 9 | Spatial wall shear stress differences. (**a**, **b**) The spatial variation of WSS at peak flow along the complete outer and inner wall for the curved and straight fistulae configurations, respectively. Note the mean WSS value at cross-sections 1 and 2 is lower for the curved (double-headed arrows) as compared to the straight configuration (double-headed arrows). Note that the absolute difference between WSS at the outer and inner walls is far greater for the straight as compared to the curved configuration at sections 1 and 2.

and 2, which are 3 and 2.7 cm from the AV anastomosis, are indicated with dotted lines in Figure 9.

Similar differences in absolute WSS values can also be seen at a location close to the AV anastomosis (1.1 cm) and at the vein outlet location, which is 5.5 cm from the AV anastomosis. At both these locations, the absolute difference in WSS values is greater in the straight configuration as compared to the curved configuration (compare the double-headed arrows for the straight configuration in Figure 9b with the double-headed arrows for the curved configuration in Figure 9a).

Identification of histological differences between the curved and straight AV fistulae and correlations with differences in WSS

Representative sections of the PV from the curved and straight configurations are shown in Figures 10a and 10b, respectively. We focused our attention on the PV because it is the region of maximal stenosis in our pig model.[17] The double-headed arrows in Figure 10a and b denotes the intima-media thickening in the PV regions of curved and straight configurations of the AV fistula. It can be observed that the straight configuration (Figure 10b) has an eccentric

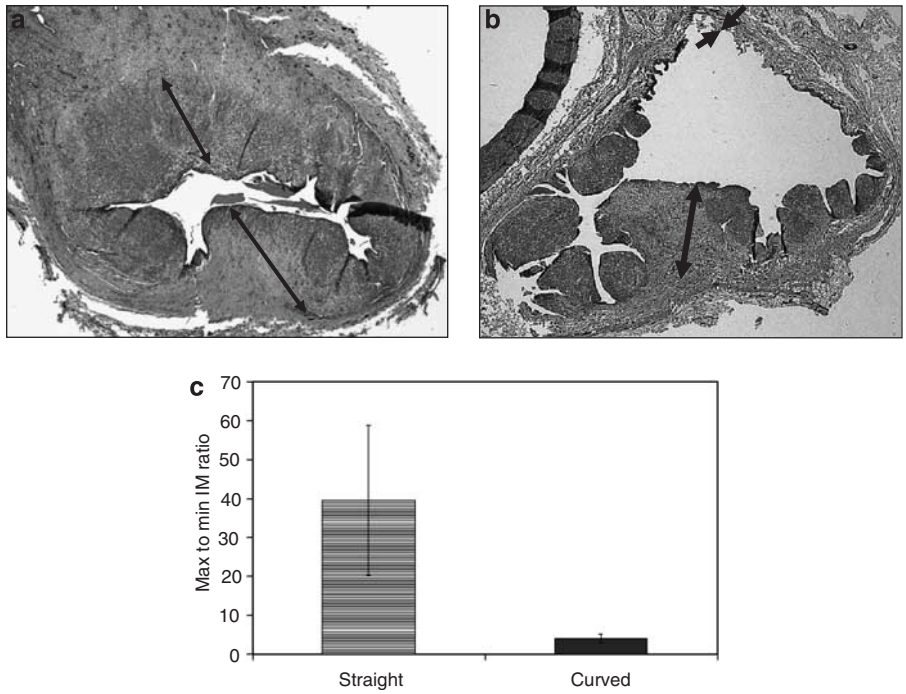

Figure 10 | Histological correlation of curved and straight fistulae. Immunohistochemical stains of (**a**) curved and (**b**) straight fistula at 42 days postsurgery are shown. (**c**) Shows the ratio of maximum to minimum intima-media thickness for the straight and curved fistulae, respectively. Note that the greater differences in wall shear stress seem to have translated into histological differences.

pattern of intima-media thickening, whereas the curved configuration has a far more uniform pattern of intima-media thickening in the PV (Figure 10a).

Figure 10c documents the mean maximum to minimum intima-media thickening ratio in the straight as compared to the curved configurations. A high value (ratio = 40) of maximum to minimum intima-media thickening ratio (denoting an eccentric pattern of thickening) is present for the straight configuration as compared to a very low ratio in the curved configuration (ratio = 4), indicating a uniform pattern of intima-media thickening.

These results suggest that the greater differences in WSS between the outer and inner walls of the straight AV fistula could have translated into the eccentric pattern of intima-media thickening seen in the straight AV fistula.

DISCUSSION

We have performed, for the first time, a CFDs analysis of an *in vivo* pig AV fistula. Although, previous CFD analyses have been performed in the context of AV grafts and fistulae, they have primarily been *ex vivo* models that have focused on reconstructed AV fistulae and grafts.[18–20] Ene-Iordache *et al.*[21] have used digital subtraction angiography to develop a complete WSS profile of a radiocephalic AV fistula in a dialysis patient, but such studies obviously cannot have histological correlations. We believe that the ability to develop a complete hemodynamic profile of an *in vivo* AV access in an animal model could allow us to dissect out the linkages between hemodynamic (WSS), histological (luminal stenosis and intima-media thickening) and future clinical (fistula maturation and thrombosis) parameters. The key findings from our study are discussed below.

Linkages between hemodynamic WSS and intima-media thickening in the curved model

An important finding of this study was the documentation of WSS in different regions of the venous segment of the AV fistula at the time of surgery, with a decreasing trend of 'mean' WSS from the AV anastomosis to the PV. Previous studies have suggested a number of mechanisms by which WSS could influence the biology of vascular stenosis.[11] Thus, high and moderate WSS has been associated with good endothelial function, a reduced expression of adhesion molecules, an increased expression of endothelial nitric oxide synthase and a reduction in oxidative stress In contrast low WSS has been linked to endothelial dysfunction, reduced nitric oxide production, increased oxidative stress and atheroma/neointima formation and also a propensity to vasoconstriction rather than vasodilatation.[22,23] In addition, low WSS has traditionally been thought to result in the deposition of cellular and protein elements onto the vessel wall which could then predispose to neointima or atheroma formation.[24,25]

In our studies, we found that there was an inverse correlation between 'mean' WSS at the time of AV fistula placement and the degree of luminal stenosis (intima-media thickening) at 42 days postsurgery. However, it must be pointed out that the hemodynamic measurements and the histological studies were performed in different animals. This is in keeping with the generally accepted hypothesis (see

above) on the linkage between WSS and vessel wall thickening. However, it is important to emphasize that the WSS levels in our AV fistula model were extremely high and that such high levels have been linked to endothelial damage/dysfunction as well.[26] Indeed, Hofstra *et al.*[27,28] have demonstrated that high flow rather than low flow correlates with AV stenosis. However the overall inverse correlation between WSS and intima-media thickening suggests that low WSS correlates with vascular stenosis in our AV fistula model.

Validation of our technique for deriving a WSS profile for a new anatomical configuration

The above-described linkage between WSS and luminal stenosis would suggest that the greater difference in 'derived' WSS between the outer and inner walls of the straight AV fistula should result in a more eccentric pattern of intima-media thickening. The fact that this did in fact occur, strongly validates our initial hypothesis about the linkages between WSS and intima-media thickening and also the CFD technique that we used to 'derive' a WSS pattern for a straight AV fistula from a calculated WSS in a curved AV fistula using actual *in vivo* measurements. Though, it is quite reasonable to assume that there might be differences in the WSS values as a result of changing the anatomical configuration, this study aims to quantify the differences between the configurations, which has not been carried out so far. We believe that this result has great clinical relevance as it could be possible to use this technique to identify 'ideal' anatomical configurations with consequent 'ideal' WSS profiles for individual patients.

Clinical impact of the described CFD analysis on hemodialysis vascular access dysfunction

In summary, we have presented a description of a detailed hemodynamic profile in a large animal AV fistula model. We have also demonstrated our ability to alter the original curved AV fistula model to a modified anatomical configuration of an AV fistula, using an original template derived from an actual *in vivo* AV fistula in our pig model through computer-modeling techniques. Although there are still gaps in our understanding of the exact linkages between WSS and clinical AV fistula success or failure, we believe that the development of computer-modeling techniques, such as those described above, could be an important step toward the optimization of the anatomical configuration of individual AV fistulae prior to surgery. In particular, the described techniques for deriving a WSS profile for the straight configuration could be used to develop computer models of an ideal or near-ideal anatomical configuration for individual patients by feeding in data on the arterial and venous anatomy for specific patients. An ideal anatomical configuration would result in minimization of regions of low WSS. In addition, we speculate that those anatomical configurations which minimize low WSS regions will also be those that are able to achieve maximal venous segment dilatation with minimal stenosis, that is, successful maturation with long-term patency. Thus, the future clinical application of the techniques described in this study could be an important part of a multipronged approach to improve both AV fistula maturation and long-term patency. We are cognizant of the fact that at a clinical level it can sometimes be difficult to create an exact replica of a computer-modeled configuration, hence the use of the term 'near ideal'. However, we are also aware of the possible future availability of devices that should make it possible to create AV fistulae in any anatomical configuration. We therefore truly believe that these results could have important clinical significance. We also believe that further research using the techniques described above, will allow us to dissect out the linkages between hemodynamic profiles, molecular signaling, histological patterns, and clinical AV fistula maturation/stenosis.

MATERIALS AND METHODS

Pig model development

A total of two curved AV fistulae and four straight AV fistulae were placed as previously described in our pig model of AV fistula stenosis.[17] Briefly, an end to side anastomosis in either a curved or straight configuration was created between the femoral artery and femoral vein, in a 50 kg Yorkshire Cross pig (Figure 1). Animals were killed at 42 days postsurgery and the entire AV fistula was carefully dissected out and processed as below. Anatomical and hemodynamic measurements were performed in a curved AV fistula animal.

Histological studies

The dissected venous segment was fixed in formalin for 24 h, coated with paraffin and then divided into 4 mm blocks. The blocks were embedded in paraffin and sectioned into 4-μm-thin sections. The sections were then stained for the expression of smooth muscle α-actin using a standard streptavidin biotin immunohistochemical technique. For the purpose of the histological analysis, the entire venous segment from the curved AV fistulae was divided into four different anatomical regions PV, jJuxtaanastomotic segment, venous portion of the AV anastomosis (AV-V), and arterial portion of the AV anastomosis (AV-A) as previously described.[17] Percentage luminal stenosis for the curved AV fistulae was calculated as previously described[17] within different regions of the AV fistula using standard histomorphometric techniques (Image J software, 1.35 P; NIH). In brief, the values for percentage luminal stenosis for all the blocks within a specific region were averaged to get a value for percentage luminal stenosis for each fistula. Values for all four curved fistulae were then averaged to get a value for each anatomical region. An identical analysis was carried out on the straight AV fistulae. In addition, PV sections from both the curved and straight AV fistulae were specifically assessed for the ratio of maximal intima-media thickness to minimal intima-media thickness. We paid particular attention to this measurement as the derived WSS values for the straight AV fistulae (see below) suggested that there should be a difference in this particular histological parameter.

Assessment of anatomical configuration and internal diameter for the curved AV fistulae

This was carried out through an IVUS and angiographic evaluation. IVUS analysis was performed with a Clear View Ultra IVUS Machine (Boston Scientific Corporation, Natick, MA, USA). Briefly,

an Atlantis 40 MHz, 2.9 F, IVUS catheter (Boston Scientific Corporation) was directed into the PA under direct vision at the time of fistula placement. IVUS recordings of the PA, the arterial side of the AV anastomosis and the DA were performed using a constant-speed pullback technique, with measurements being made every 1–3 mm. Measurements were performed over a 60 mm distance from the PA to DA. The IVUS catheter was then passed under direct vision, across the AV anastomosis and serial measurements of the venous limb of the AV fistula were performed, starting approximately 50 mm proximal to the AV anastomosis. In order to obtain the anatomical configuration (curvature) of the AV fistula a standard angiogram was performed following fistula placement.

Flow and pressure measurements

Blood flow was measured in the PA, DA, and PV of the curved AV fistula configuration using perivascular flow probes (Transonic Systems Inc., Ithaca, NY, USA). Although flow was measured in all the three of the above locations (PA, DA, and PV), we only used the flow data from the PA and DA to perform the computational analyses. These values provided us with adequate input boundary condition to perform the hemodynamic wall shear stress calculations and so are the only ones shown in Figure 2. As a measure of crosscheck, the computed venous flow was validated with the measured flow in the vein. In order to obtain a pressure outlet boundary condition and also for the purposes of validation of the CFD model, blood pressure within the AV fistula was measured at the PA and within the venous segment (on day 2) by placing a 6F catheter at these sites and connecting this to an external pressure sensor linked to a Combo Map machine (Volcano Therapeutics, Rancho Cordova, CA, USA).

Development of a complete WSS profile for the curved AV fistulae

The recorded cross-sectional IVUS images of the entire curved AV fistula were extracted from the video casette recordings and digitized. As the IVUS images contained only two-dimensional information, the images were stacked so that the centroids of all the images were aligned on a straight line for the arterial side. On the venous side of the AV fistula, the centroids of the images were oriented based on angiographic images of the AV fistula, in order to recreate the curved venous segment. Surface and curve fit to the polylines were then incorporated. A three-dimensional AV fistula geometry was reconstructed with tetrahedral elements. This three-dimensional mesh was then used to derive WSS using finite volume method[15,16] (Fluent; Version 6.3.26). Specifically, the flow data from the perivascular probe measurements was applied to the inlet and outlet of the PA and DA, respectively. The measured venous pressure pulse was applied at the outlet of the PV to compute the PA pressure for validation purposes.

To give a closed form solution, only three parameters are needed. Figure 2c explains the boundary conditions that were applied to our AV fistula model to calculate the WSS profile. The PA, DA, and PV of AV fistula where the hemodynamic measurements were carried out are shown in Figure 2c. The arrows indicate the flow direction. In this AV fistula configuration, at the PA and PV locations, both transient pressure and flow pulses were measured: P_1, Q_1 at PA and P_3, Q_3 at PV, whereas only transient flow pulse was measured at DA (Q_2). As mentioned earlier, only three parameters are required to perform CFDs calculation. Hence, we used only transient Q_1, Q_2, and P_3 pulses in order to generate the hemodynamic wall shear stress profile.

Derivatization of a complete WSS profile for a straight AV fistula from the calculated WSS data for the curved AV fistula

We derived a WSS profile for a straight AV fistula in order to demonstrate that it is possible to derive a WSS profile for any potential AV fistula configuration from data on vessel diameters and flow. In order to generate an AV fistula configuration with a minimized venous curvature, the inner and outer curves at a particular cross-section starting from the AV anastomosis of the curved configuration were revolved such that the curvature length was reduced, keeping the diameter nearly unchanged. The sections were then oriented in such a way that the centroids of all the cross-sections were aligned. This resulted in a three-dimensional tetrahedral mesh with close to 384,000 active cells. Finally, we introduced into this straight configuration, the same flow parameters that we had obtained *in vivo*, for the curved configuration and similar boundary conditions that we had applied to our curved configuration, in order to obtain a complete derived WSS for a straight AV fistula configuration (see Figure 6 in the Results section).

DISCLOSURE

All the authors declared no competing interests.

REFERENCES

1. Beasley C, Rowland J, Spergel L. Fistula first: an update for renal providers. *Nephrol News Issues* 2004; **18**: 88–90.
2. Beathard GA. Strategy for maximizing the use of arteriovenous fistulae. *Semin Dial* 2000; **13**: 291–296.
3. DOQI. III. NKF-K/DOQI Clinical Practice Guidelines for Vascular Access: update 2000. *Am J Kidney Dis* 2001; **37**(1 Suppl 1): S137–S181.
4. Hemphill H, Allon M, Konner K *et al.* How can the use of arteriovenous fistulas be increased? *Semin Dial* 2003; **16**: 214–223.
5. Allon M, Robbin ML. Increasing arteriovenous fistulas in hemodialysis patients: problems and solutions. *Kidney Int* 2002; **62**: 1109–1124.
6. Nasser G, Nguyen B, Rhee E *et al.* Endovascular treatment of the 'failing to mature' arteriovenous fistula. *Clin J Am Soc Nephrol* 2006; **1**: 275–280.
7. Beathard GA. Angioplasty for arteriovenous grafts and fistulae. *Semin Nephrol* 2002; **22**: 202–210.
8. Beathard GA, Arnold P, Jackson J *et al.* Aggressive treatment of early fistula failure. *Kidney Int* 2003; **64**: 1487–1494.
9. Roy-Chaudhury P, Arend L, Zhang J *et al.* Neointimal hyperplasia in early arteriovenous fistula failure. *Am J Kidney Dis* 2007; **50**: 782–790.
10. Van Tricht I, De Wachter D, Tordoir J *et al.* Hemodynamics and complications encountered with arteriovenous fistulas and grafts as vascular access for hemodialysis: a review. *Ann Biomed Eng* 2005; **33**: 1142–1157.
11. Konner K, Nonnast-Daniel B, Ritz E. The arteriovenous fistula. *J Am Soc Nephrol* 2003; **14**: 1669–1680.
12. Corpataux JM, Haesler E, Silacci P *et al.* Low-pressure environment and remodelling of the forearm vein in Brescia-Cimino haemodialysis access. *Nephrol Dial Transplant* 2002; **17**: 1057–1062.
13. Asif A, Roy-Chaudhury P, Beathard G. Early arteriovenous fistula failure: a logical proposal for when and how to intervene. *Clin J Am Soc Nephrol* 2006; **1**: 332–339.
14. Mattsson EJ, Kohler TR, Vergel SM *et al.* Increased blood flow induces regression of intimal hyperplasia. *Arterioscler Thromb Vasc Biol* 1997; **17**: 2245–2249.
15. Rajamohan D, Banerjee RK, Back LH *et al.* Developing pulsatile flow in a deployed coronary stent. *J Biomech Eng* 2006; **128**: 347–359.
16. Banerjee RK, Devarakonda SB, Rajamohan D *et al.* Developed pulsatile flow in a deployed coronary stent. *Biorheology* 2007; **44**: 91–102.
17. Wang Y, Krishnamoorthy M, Banerjee R *et al.* Venous stenosis in a pig arteriovenous (AV) fistula model: anatomy, mechanisms and cellular phenotypes. *Nephrol Dial Transplant* 2008; **23**: 525–533.
18. Sivanesan S, How TV, Black RA *et al.* Flow patterns in the radiocephalic arteriovenous fistula: an *in vitro* study. *J Biomech* 1999; **32**: 915–925.
19. Loth F, Jones SA, Zarins CK *et al.* Relative contribution of wall shear stress and injury in experimental intimal thickening at PTFE end-to-side arterial anastomoses. *J Biomech Eng* 2002; **124**: 44–51.

20. Loth F, Fischer PF, Arslan N *et al.* Transitional flow at the venous anastomosis of an arteriovenous graft: potential activation of the ERK1/2 mechanotransduction pathway. *J Biomech Eng* 2003; **125**: 49–61.
21. Ene-Iordache B, Mosconi L, Remuzzi G *et al.* Computational fluid dynamics of a vascular access case for hemodialysis. *J Biomech Eng* 2001; **123**: 284–292.
22. Lehoux S, Castier Y, Tedgui A. Molecular mechanisms of the vascular responses to haemodynamic forces. *J Intern Med* 2006; **259**: 381–392.
23. Harrison DG, Widder J, Grumbach I *et al.* Endothelial mechanotransduction, nitric oxide and vascular inflammation. *J Intern Med* 2006; **259**: 351–363.
24. Worth Longest P, Kleinstreuer C. Comparison of blood particle deposition models for non-parallel flow domains. *J Biomech* 2003; **36**: 421–430.
25. Honda HM, Hsiai T, Wortham CM *et al.* A complex flow pattern of low shear stress and flow reversal promotes monocyte binding to endothelial cells. *Atherosclerosis* 2001; **158**: 385–390.
26. Fry DL. Acute vascularendothelial changes associated with increased blood velocity gradients. *Circ Res* 1968; **22**: 165–197.
27. Hofstra L, Bergmans DC, Leunissen KM *et al.* Prosthetic arteriovenous fistulas and venous anastomotic stenosis: influence of a high flow velocity on the development of intimal hyperplasia. *Blood Purif* 1996; **14**: 345–349.
28. Hofstra L, Bergmans DC, Leunissen KM *et al.* Anastomotic intimal hyperplasia in prosthetic arteriovenous fistulas for hemodialysis is associated with initial high flow velocity and not with mismatch in elastic properties. *J Am Soc Nephrol* 1995; **6**: 1625–1633.